Available online at www.sciencedirect.com
ScienceDirect
Journal of Solid State Chemistry 180 (2007) 2682–2689
JOURNAL OF SOLID STATE CHEMISTRY
www.elsevier.com/locate/jssc

Evolution of titania nanotubes-supported WO_x species by *in situ* thermo-Raman spectroscopy, X-ray diffraction and high resolution transmission electron microscopy

M.A. Cortes-Jácome, C. Angeles-Chavez, M. Morales, E. López-Salinas, J.A. Toledo-Antonio*

Molecular Engineering Program, Instituto Mexicano del Petróleo. Eje Central Lázaro Cárdenas 152, 07730 México, Distrito Federal, Mexico

Received 17 May 2007; received in revised form 12 July 2007; accepted 15 July 2007
Available online 26 July 2007

Abstract

Structural evolution of WO_x species on the surface of titania nanotubes was followed by *in situ* thermo-Raman spectroscopy. A total of 15 wt% of W atoms were loaded on the surface of a hydroxylated titania nanotubes by impregnation with ammonium metatungstate solution and then, the sample was thermally treated in a Linkam cell at different temperatures in nitrogen flow. The band characteristic of the W=O bond was observed at 962 cm^{-1} in the dried sample, which vanished between 300 and 700 °C, and reappear again after annealing at 800 °C, along with a broad band centered at 935 cm^{-1}, attributed to the v_1 vibration of W=O in tetrahedral coordination. At 900 and 1000 °C, the broad band decomposed into four bands at 923, 934, 940 and 950 cm^{-1}, corresponding to the symmetric and asymmetric vibration of W=O bonds in Na_2WO_4 and $Na_2W_2O_7$ phases as determined by X-ray diffraction and High resolution transmission electron microscopy (HRTEM). The structure of the nanotubular support was kept at temperatures below 450 °C, thereafter, it transformed into anatase being stabilized at temperatures as high as 900 °C. At 1000 °C, anatase phase partially converted into rutile. After annealing at 1000 °C, a core–shell model material was obtained, with a shell of *ca.* 5 nm thickness, composed of sodium tungstate nanoclusters, and a core composed mainly of rutile TiO_2 phase.

Keywords: Titania nanotubes; Tungsten; Anatase; Raman spectroscopy; Transmission electron microscopy

1. Introduction

Tungsten oxide loaded on supports such as Al_2O_3, SiO_2, ZrO_2 and TiO_2 are known to be catalytically active for several industrially important reactions, including *n*-alkanes isomerization, alcohol dehydrogenation, oxidative desulfurization (ODS), cracking, olefin metathesis, NO_x reduction and hydrocarbons alkylation [1–10]. Particularly, WO_x/TiO_2 catalysts are used industrially for selective catalytic reduction of NO_x by ammonia in exhaust gases, olefins conversions and oxidation reactions [11,12], since this catalytic system combines acidic, redox and photocatalytic properties. These catalysts are prepared with commercially available TiO_2 supports, which limit the tungsten content to 10% of WO_3 for monolayer coverage, due to the low specific surface area of the support. In order to increase the amount of WO_3 loading at the monolayer level, Eibl et al. used the oxyhydroxide precursor of titania support, obtaining two different tungstate species on the surface of TiO_2 [13]. One is a three-dimensional tungsten structure and the other one is tungsten species strongly bonded to TiO_2 support, probably forming Ti–O–W linkages. Catalytic activity upon *n*-pentane isomerization reaction resembles that showed by tungstated zirconia catalysts [14], and there is apparently no difference between catalysts prepared starting with a crystallized or amorphous oxyhydroxide titania support [14,15].

In spite of many interesting catalytic properties of WO_x/TiO_2 system, practically all the attention has been focused on

*Corresponding author.
E-mail address: jtoledo@imp.mx (J.A. Toledo-Antonio).

0022-4596/$ - see front matter © 2007 Elsevier Inc. All rights reserved.
doi:10.1016/j.jssc.2007.07.012

the characterization of WO_x/ZrO_2, and WO_x/Al_2O_3, while only a few studies concerning WO_x/TiO_2 system have been reported, probably due to the usually low initial specific surface area (SSA), typical of TiO_2. To overcome the disadvantages of low SSA in conventional TiO_2, titanium oxide in anatase phase has been converted into titania nanotubes or nanofibers through a relatively simple alkaline hydrothermal method [17,18]. The large external surface and internal volume of the nanotubes make it possible to disperse a large amount of transition metal oxides (porosity exceeds 0.5 cm^3/g) [19,20]. The synthesis, properties, and applications of protonated titanates and TiO_2 nanostructured materials have been recently reviewed by Bavykin et al. [21] and Chen and Mao [22]. The nanotubes disperse efficiently Pd, Zn, Au, CdS and Ru nanoparticles, generating materials with multiple potential applications in catalysis, photocatalysis, electrocatalysis, photovoltaic cells, lithium batteries, hydrogen storage and separation, etc. [21]. Recently, we have reported the use of a hydrous titania with nanotubular morphology as an efficient support for the dispersion of a high amount of WO_x species on the surface [16]. When nanotubular structure collapse, residual Na^+ ions are released and react with WO_x species changing the coordination of the later from octahedral to tetrahedral. The obtained surface sodium tungstate particles were highly active for oxidation of dibenzothiophene [16].

In this work, the structural evolution of WO_x species, initially impregnated on a TiO_2 with nanotubular morphology, was followed by *in situ* thermo-Raman spectroscopy in a Linkam cell. The sample obtained after thermal treatment at 1000 °C was characterized by X-ray diffraction and electron microscopy (HRTEM and HAADF-STEM).

2. Experimental

2.1. Preparation of titania supports

Titania with nanotubular morphology was synthesized by a hydrothermal treatment of Hombitec K anatase TiO_2 provided by Sachtleben Chemie GmbH. Forty-five grams of anatase powder were suspended in 3 L of an aqueous 10 M NaOH solution and the resulting suspension was placed in an autoclave. The hydrothermal reaction was conducted at 100 °C, for 18 h under stirring at 200 rpm. Then, the white slurry was filtered and neutralized with a 1 M HCl solution until the pH was lowered to 3.0. The resulting suspension was maintained at this pH overnight under continuous stirring. The material was repeatedly washed with abundant deionized water until it was chlorine-free, i.e. by testing with a silver nitrate solution. The material was finally dried at 100 °C overnight, yielding a hydrous titania powder with nanotubular morphology.

2.2. Preparation of WO_x/TiO_2

Impregnation of tungsten species over hydrous nanotubular titania was achieved by an aqueous impregnation method. Twenty-two grams of the support were placed in contact with an excess (6 ml/g) of an aqueous ammonium metatungstate $[(NH_4)_6H_2W_{12}O_{40}]$ solution (0.036 M) in order to obtain 15 wt% W loaded on the support. The pH was adjusted to 10 with a few drops of ammonium hydroxide. The slurry was left for 1 h at room temperature, and then excess water was eliminated at 100 °C, in a rotary evaporator. Finally, the resulting material was placed in an oven at 100 °C overnight.

2.3. Characterization

2.3.1. Raman spectroscopy

The Raman spectra were recorded using a Jobin Yvon Horiba (T64000) spectrometer, equipped with a confocal microscope (Olympus, BX41) with an argon ion laser operating at 514.5 nm at a power level of 10 mW. The spectrometer is equipped with a CCD camera detector. A total of 20 mg of dried powdered WO_x/titania nanotubes were placed in a Linkam cell directly adapted to the microscope of the instrument; the cell allows the use of controlled atmosphere and temperature. The glass window of the cell was 1 mm thick. The sample was heated at 10 °C/min rate in 100 cm^3/min of nitrogen flow up to the command temperature, then, it remained at this temperature for 10 min. Thereafter, the sample was cooled at 20 °C/min by means of a recirculation cooling bath and then spectra were recorded. This procedure was repeated for each temperature. A nitrogen atmosphere was used throughout all measurements.

2.3.2. X-ray diffraction

A sample previously annealed at 1000 °C during the *in situ* thermo-Raman study was transferred into a packed glass holder and analysed by X-ray diffraction (XRD). The XRD was recorded at room temperature with Cu$K\alpha$ radiation in a Bruker Advance D-8 diffractometer having θ–θ configuration and a graphite secondary-beam monochromator. Diffraction intensity was measured in the 2θ range between 15° and 80°, with a 2θ step of 0.02° for 3 s per point.

2.3.3. Transmission electron microscopy

High resolution transmission electron microscopy (HRTEM) and scanning transmission electron microscopy (STEM) analysis of a sample annealed at 1000 °C in the thermo-Raman cell was performed in JEM-2200FS transmission electron microscope with accelerating voltage of 200 kV. The microscope is equipped with a Schottky-type field emission gun and an ultra high resolution (UHR) configuration (Cs = 0.5 mm; Cc = 1.1 mm; point to point resolution = 0.19 nm) and in-column omega-type energy filter. STEM is particularly useful in studies of nanoparticles when a high angle annular dark field (HAADF) detector, which collects electrons that undergo Rutherford scattering, is used. Images can then be acquired where the intensity is approximately proportional to Z^2 (Z is the atomic number of the scattering atom). Therefore, elements

with a high Z produce higher intensity and white contrast images. The technique is useful to disclose the presence of different chemical elements when they have a big difference in atomic numbers, as encountered in supported catalysts. Local and line scan chemical analysis by energy dispersive X-ray spectrometry (EDXS) was performed in a NORAN energy dispersive X-ray spectroscope. The samples were ground, suspended in isopropanol at room temperature, and dispersed with ultrasonic agitation; then, an aliquot of the solution was dropped on a 3 mm diameter carbon film supported on a lacey copper grid.

3. Results and discussion

Raman spectra of the titania nanotubes used as support and that of the impregnated sample are presented in Fig. 1. The Raman spectra of titania nanotubes used as support are made up of three main characteristic bands at 274, 450 and 697 cm^{-1}, and other less intense bands at 194, 386, 830 and 905 cm^{-1}. After impregnation, an additional band was observed at 962 cm^{-1} which has been assigned to terminal W═O vibration [23]. After annealing between 300 and 400 °C, the band of W═O extinguished, and only the three main vibrating bands, characteristic of the titania nanotubes, were observed at ~280, 450 and ~700 cm^{-1}. After annealing at 450 °C, anatase active modes at 149, 200, 396, 510, 636 cm^{-1} appeared in between those of the nanotubes indicating that nanotubular structure initiate their transformation back into anatase at this temperature. In fact, WO_x species play a stabilizing role on the nanotubular structure, which otherwise transforms into anatase at 250 °C, in inert atmosphere [24]. When the

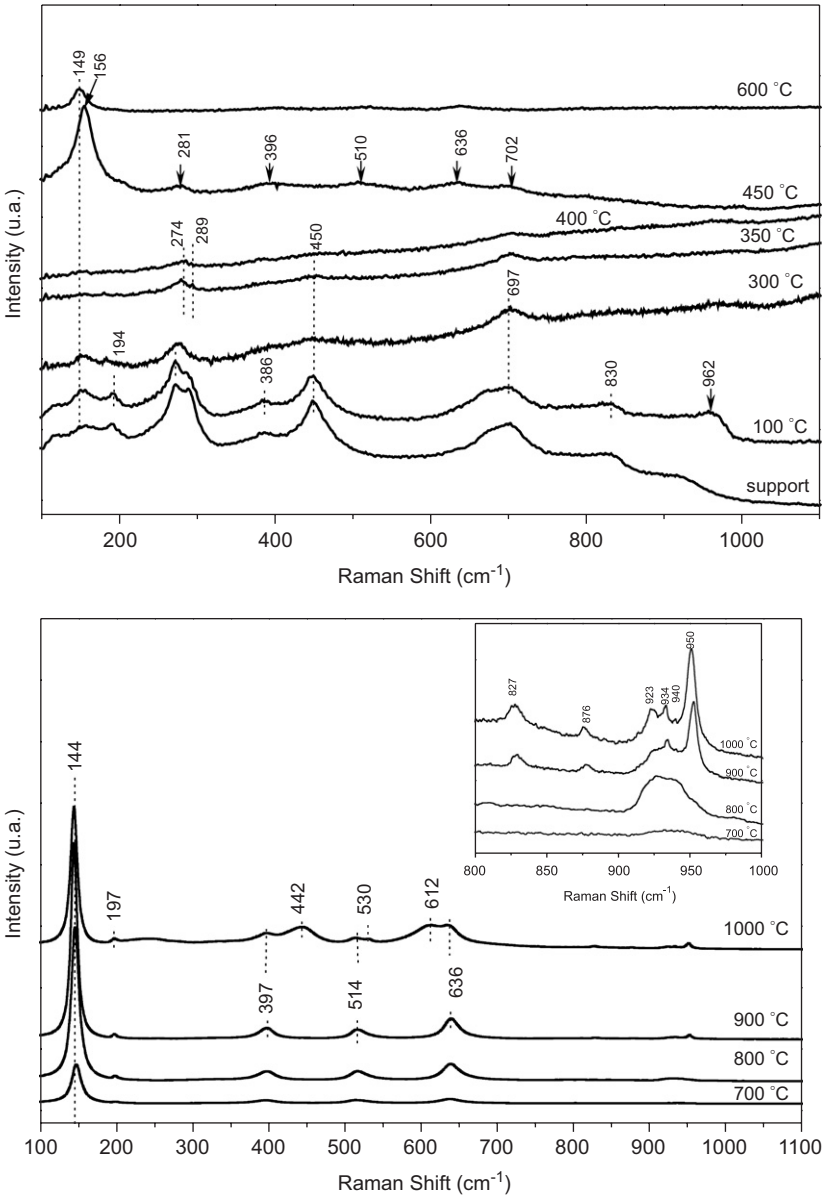

Fig. 1. Thermo-Raman spectra of titania nanotubes (support) and those of WO_x/TiO_2 from room temperature to 600 °C. Thermo-Raman spectra of WO_x/TiO_2 from 700 to 1000 °C.

sample was annealed at 600 °C, only anatase modes were observed, suggesting a complete transformation of the nanotubular structure, however, the intensity of the peaks was low compared with that in the sample annealed at 450 °C. In fact, only the active E*g* peak was evident with a shift towards low frequencies, e.g. from 156 to 149 cm^{-1} after annealing at 450 and 600 °C, respectively. The variation in intensity and position of anatase E*g* mode may indicate a surface reaction between tungsten species and the support at this temperature, as no evidence of any terminal W═O was distinguished in the spectra range between 900 and 1000 cm^{-1}; where the spectra remained totally featureless.

After annealing at 700 °C, the intensity of the anatase active modes increased in comparison with the sample annealed at 600 °C, and a very small broad band appeared at 935 cm^{-1}, typical of terminal W═O in tetrahedral coordination, as shown in Fig. 1(cntnd). At 800 and 900 °C, only the bands of the anatase phase were observed with higher intensity as annealing temperature increased. The 935 cm^{-1} band rises between 700 and 800 °C and splits into components at 923, 934, 940 and ~950 cm^{-1} for a temperature of 900 °C. These peaks correspond to the symmetric and antisymmetric vibration of terminal W═O in two different environments on the surface of anatase [23]. Two additional peaks were observed at 827 and 876 cm^{-1}, which correspond to bridging W–O bonds of tungsten species in different environments. The same tungsten vibrating peaks were more clearly defined when the sample was annealed at 1000 °C, in which case titania support partially transformed into rutile phase, as indicated by the peaks at 442 and 612 cm^{-1}. It is important to mention the high stabilization degree that tungsten species induce on titania anatase structure, which normally transform into rutile at 700 °C.

The resulting sample, after annealing in the Linkam cell at 1000 °C, was studied by XRD and HRTEM microscopy. From the XRD in Fig. 2, it can be observed that the sample mainly consisted of a mixture of anatase and rutile phases. Additionally, smaller peaks of other phases were evident and were identified as sodium tungstate phases, Na_2WO_4 and $Na_2W_2O_7$, having JCPDS card numbers 11-0772 and 32-1186, respectively. As titania nanotubes were obtained through a hydrothermal treatment with NaOH, a residual amount of Na^+ ions remained in the support. In fact, by EDXS on the support after annealing at 500 °C, 2.6 wt% of sodium was determined. Accordingly, sodium ions remain in the interlayer space of the nanotubes' walls [25]. From Raman spectroscopy, it was evident that after *in situ* annealing above 450 °C, the nanotubular structure partially transformed into anatase, the interlayer space in the walls disappeared and the sodium ions were released to the surface, reacting with surface WO_x species forming sodium tungstate phases. However, the tungstate species were not detected by Raman spectroscopy below 700 °C, probably because these species are strongly bonded to the TiO_2 surface or interacting with Ti atoms at two or three atomic layers from the surface yielding Ti–O–W linkages [13]. This strong interaction is produced by the annealing procedure, in the Linkam cell with N_2 flow passing through the sample during the annealing treatment. When the sample was calcined in an oven in static air, the W═O vibration appeared at 960 and 935 cm^{-1} after annealing at 400 and 500 °C, respectively, as consequence of a change in the coordination of WO_x species from octahedral to tetrahedral [16]. Therefore, the annealing procedure with a flow of N_2 hinders WO_x particles crystallization and inhibits the support transformation.

HAADF-STEM images, displayed in Fig. 3, show that the sample is formed by big gray contrast particles with dimensions of *ca.* 100 nm (B-label), covered by a thin white contrast layer (A-label). As the intensity in the image depends on the atomic number, this result suggests that the

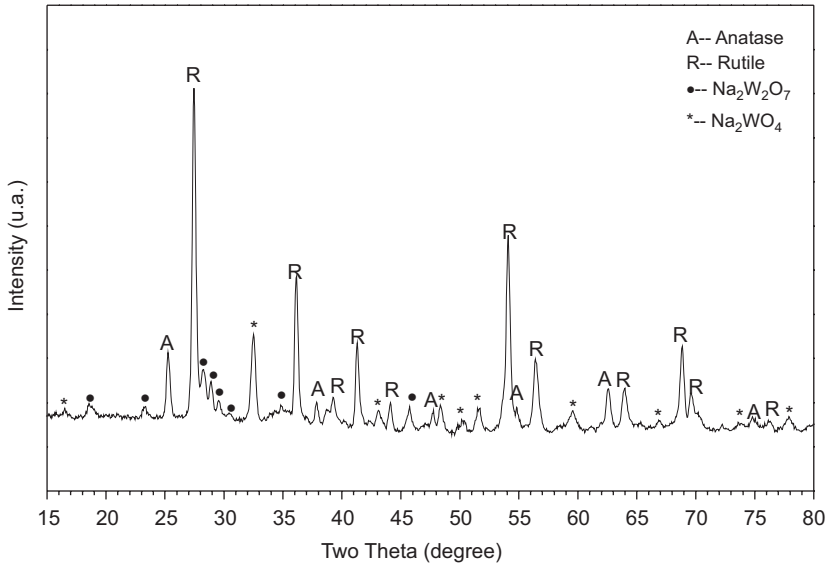

Fig. 2. XRD patterns of a WO_x/TiO_2 sample, after annealing at 1000 °C in the Raman cell.

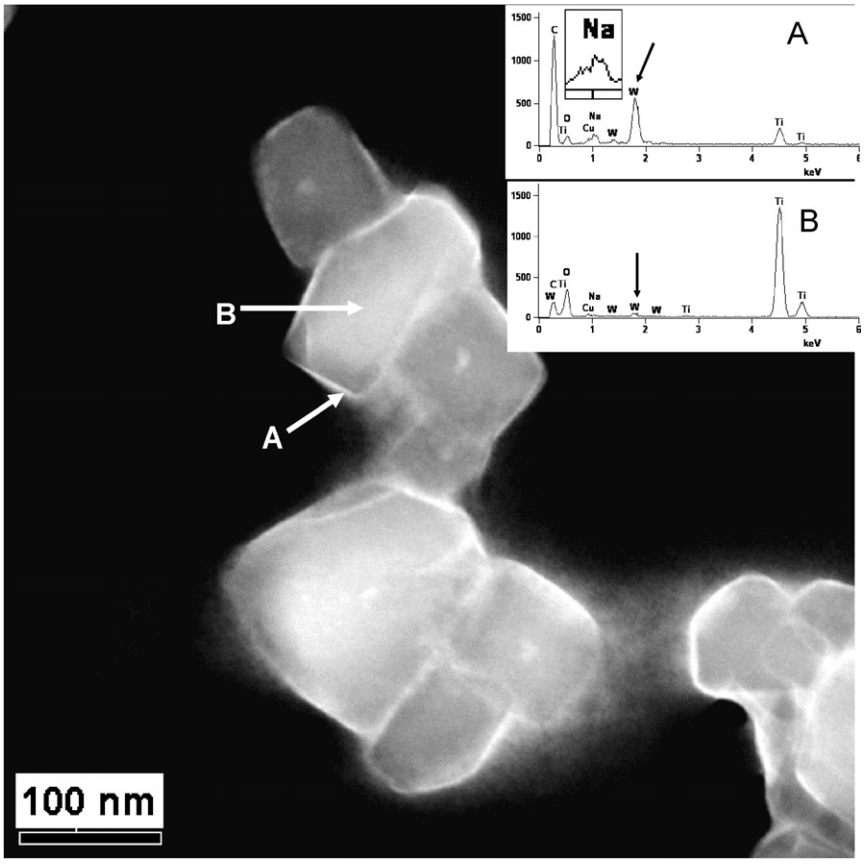

Fig. 3. HAADF-STEM image of a WO_x/TiO_2 sample, after annealing at 1000 °C in the Raman cell. Inset A: EDX spectrum of crystal's edge; Inset B: EDX spectrum of crystal's center.

thin layer is a shell formed by tungsten atoms surrounding the big gray particles, which are mainly composed by titanium atoms. This result was confirmed by the local chemical analysis performed by STEM-EDXS, which is a technique that allows having a better control of the electron beam in order to obtain a more focused chemical analysis in the particles. The results obtained are displayed as EDX spectrum inset in Fig. 3. Local analysis obtained from the white crust mainly detected tungsten atoms (EDX spectrum labeled as A), suggesting an enrichment of W atoms in the thin layer, which surrounded all big particles. Here, it is not possible to assure that titanium atoms detected correspond to the thin layer. Although the EDXS system can be used as a sub-nanometer probe, the local chemical analysis usually contains some background signal from surrounding areas, then, detected Ti atoms are likely to belong to the big gray particles of the support. Notice that, in addition to the W atoms, the white thin layer contains an appreciable amount of Na atoms. On the other hand, chemical analysis performed in the flat region of the big particles (EDX spectrum labeled as B), clearly revealed that they are rich in Ti atoms (e.g. high intensity Ti peaks in the EDX spectrum), and only a little W-associated signal was detected.

More direct evidence of the W-rich thin layer is shown in the EDXS line profile, drawn through the particle in the HAADF-STEM image in Fig. 4. When the acquired signal was near to the edge of the particle surface, the W profile was intense, obtaining a maximum value which correspond to the thickness of the W-rich crust, and further beyond the edge, the intensity of W signal dropped as observed in the W profile. In the other hand, titanium concentration decreased towards the particle surface. Hence, from the HAADF-STEM and STEM-EDXS results we can conclude that the titanium particles are covered by a thin layer of W and Na atoms, which may correspond to the sodium tungstate phases.

The presence of ~3 nm nanoparticles deposited on the crystalline surface of the large particles was detected by HRTEM, as shown in Fig. 5. The nanoparticle size suggests that only one-nanoparticle layer was deposited on the large particle surface, as shown in black contrast in HRTEM image. The structural analysis carried out in the lattice of the large particle revealed *d*-spacing of 0.327, 0.323 and 0.258 nm corresponding to the $(1\,{-}1\,0)$, $(0\,1\,1)$ and $(1\,0\,1)$ planes in the $[1\,{-}1\,{-}1]$ direction of the rutile tetragonal phase, according to the 21-1276 JCPDS card and the crystallographic analysis of the FFT pattern (see inset C in Fig. 5). The nanoparticles that were very well separated from the large particle surface were also structurally analyzed to identify the tungsten compound type. The first nanoparticle marked as A in the black arrow

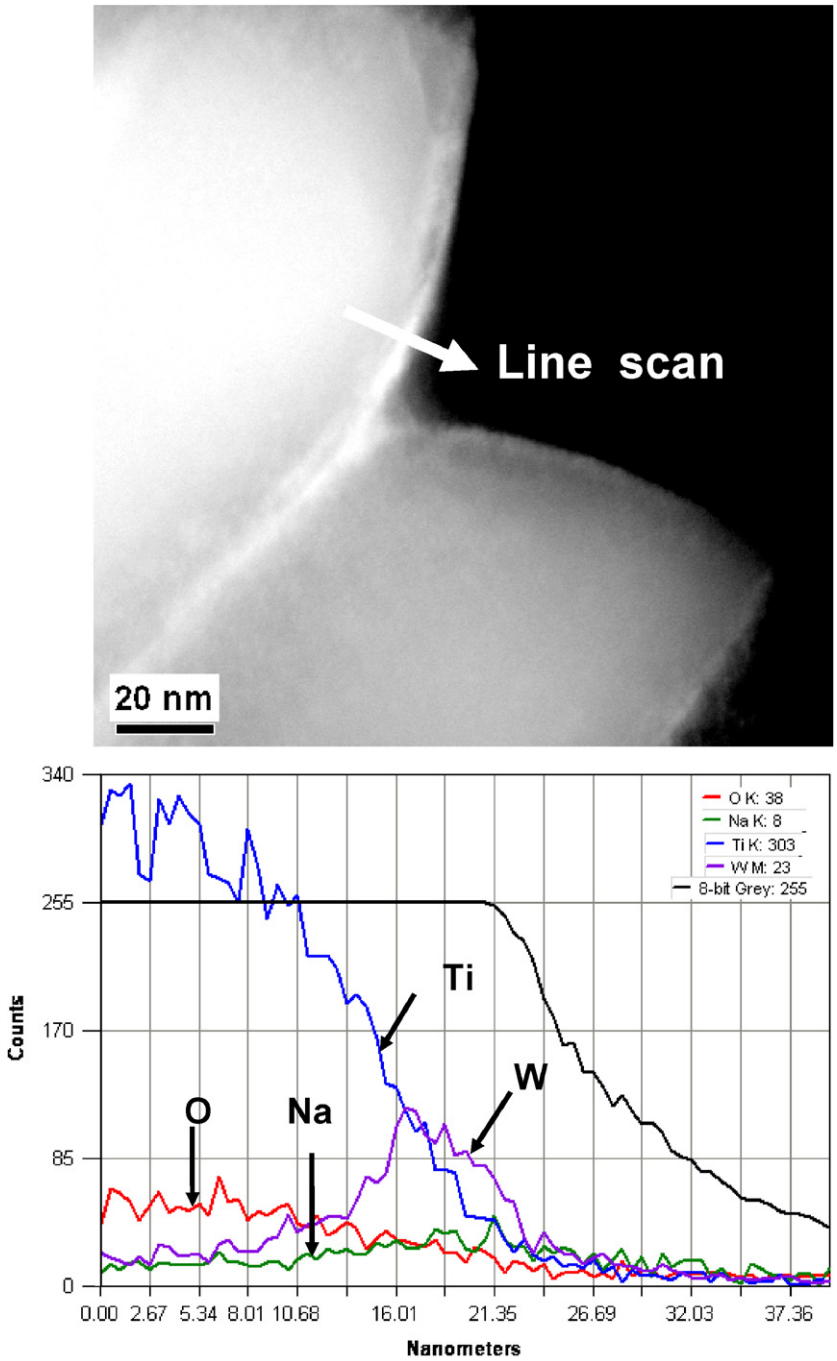

Fig. 4. HAADF-STEM image of a WO_x/TiO_2 sample, after annealing at 1000 °C in the Raman cell (upper image). EDXS line profile across the white arrow (lower plot).

and magnified in inset A, Fig. 5, had *d*-spacing of 0.218, 0.206 and 0.151 nm which matched very well with the *d*-spacing of the 70-0149 JCPDS card that correspond to the (2 −2 −2), (3 2 1) and (5 0 −1) planes in the [1 −4 5] direction of the cubic $Na_{0.75}WO_3$ structure. The second nanoparticle analyzed (see inset B in Fig. 5), had *d*-spacing of 0.240, 0.240 and 0.209 nm and they correspond to the (3 1 0), (0 −3 1) and (3 −2 1) planes in the [1 −3 −9] direction of cubic $Na_{0.75}WO_3$ structure. The crystalline phase of tungsten nanoparticles detected on the TiO_2 support by HRTEM does not exactly correspond to the phases detected by XRD. A plausible reason is that the nanoparticles had dimensions below 3 nm, thus, they could not be detected by XRD. Evidently, the tungstate particles in XRD have crystallite sizes higher than 5 nm, and they were not observable in the region studied by HRTEM. These results suggest that multiple sodium tungstate phases including $Na_{0.75}WO_3$, Na_2WO_4 and $Na_2W_2O_7$ were formed by a solid state reaction between the residual Na^+ ions and impregnated WO_x species after annealing at 1000 °C.

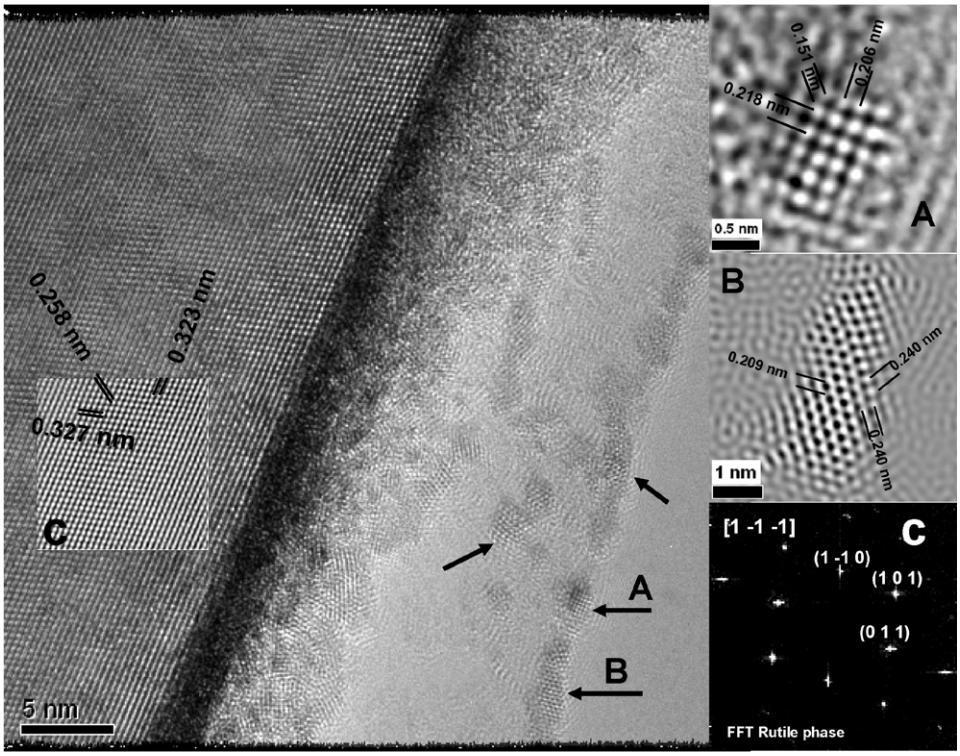

Fig. 5. HRTEM image of a WO_x/TiO_2 sample, after annealing at 1000 °C in the Raman cell. Inset A: magnification and *d*-spacings of region A. Inset B: magnification and *d*-spacings of region B. Inset C: FFT of rutile phase in region labeled as C.

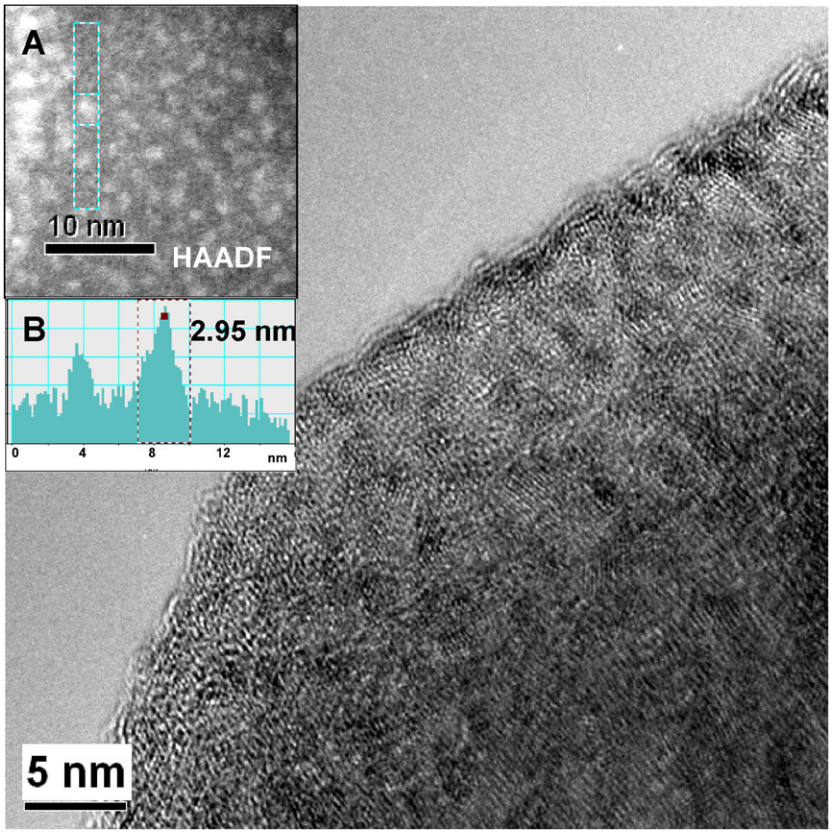

Fig. 6. HRTEM image of a WO_x/TiO_2 sample, after annealing at 1000 °C in the Raman cell. Inset A: HAADF-STEM image and inset B: intensity profile corresponding to the rectangular region marked in inset A.

In spite of the high annealing temperature, very small tungsten nanoparticles with dimensions below 3 nm scattered on the surface of TiO_2 particles were observed, as shown in dark spots in the HRTEM image of Fig. 6 and white spots in the HAADF-STEM image inset *A*. The inset *B* of Fig. 6 show the intensity profile obtained across the rectangular region in the inset A showing that tungstate particle size in this case was *ca.* 2.95 nm. These nanoparticles were quite similar to those recently observed on the surface of WO_x/ZrO_2 [26,27].

4. Conclusions

Structural evolution of WO_x (15 wt%) on nanotubular TiO_2 was followed by Raman spectroscopy by *in situ* treatment in a Linkam cell in a nitrogen atmosphere. Octahedral WO_x species were initially observed in a dried sample, thereafter, the corresponding band of W=O, at 900–1000 cm^{-1} extinguished, as a consequence of a strong interaction between WO_x and TiO_2, broadening also the characteristic bands of anatase TiO_2 phase. After annealing at 800 °C, the intensity of the peaks corresponding to anatase increased and a broad W=O signal appeared at 935 cm^{-1} from W atoms in a tetrahedral coordination. The W=O vibrations were clearly defined after annealing treatment at 1000 °C, from different sodium tungstate phases. By XRD analysis, the Na_2WO_4 and $Na_2W_2O_4$ phases were detected, whereas by HRTEM *ca.* 3 nm nanoparticles of $Na_{0.75}WO_3$ were detected on the surface of TiO_2 with a rutile structure.

The strong interaction between WO_x species and TiO_2 support stabilizes the anatase structure even at 900 and 1000 °C, it partially transforms into rutile, yielding a core–shell material with the shell composed by nanoclusters of sodium tungstate phases and the core consisting of TiO_2 rutile phase.

Acknowledgments

The financial support from IMP-D.00446 and IMP-I.00383 projects is greatly appreciated.

References

[1] M. Hino, K. Arata, J. Chem. Soc. Chem. Commun. (1987) 1259.
[2] T. Yamaguchi, Appl. Catal. A 6 (1990) 1.
[3] G. Ramis, C. Cristiani, L. Leitti, P. Forzatti, F. Bregani, Langmuir 8 (1992) 1744.
[4] C.D. Baertsch, K.T. Komala, Y.H. Chua, E. Iglesia, J. Catal. 205 (2002) 44.
[5] T. Kim, A. Burrows, C.J. Kiely, I.E. Wachs, J. Catal. 246 (2007) 370.
[6] J. Macht, C.D. Baertsch, M. May-Lozano, S.L. Soled, Y. Wang, E. Iglesia, J. Catal. 227 (2004) 479.
[7] S. Sarish, B.M. Devassy, W. Böhringer, J. Fletcher, S.B. Halligudi, J. Mol. Catal. A. 240 (2005) 123.
[8] F. Di-Grégorio, V. Keller, T. Di-Costanzo, J.L. Vignes, D. Michel, G. Maire, Appl. Catal. A 218 (2001) 13.
[9] X. Xiao, J.W. Tierney, I. Wender, Appl. Catal. A 183 (1999) 209.
[10] S.M. Kumbar, G.V. Shanbhag, F. Lefebvre, S.B. Halligudi, J. Mol. Catal. A 256 (2006) 324.
[11] L.J. Alemany, L. Lietti, N. Ferlazzo, P. Forzatti, G. Busca, E. Giamello, F. Bregani, J. Catal. 155 (1995) 117.
[12] C. van Schalkwyk, A. Spamer, D.J. Moodley, T. Dube, J. Reynhardt, J.M. Botha, Appl. Catal. A 255 (2003) 121.
[13] S. Eibl, B.C. Gates, H. Knözinger, Langmuir 17 (2001) 107.
[14] S. Eibl, R.E. Jentoft, B.C. Gates, H. Knözinger, Phys. Chem. Phys. Chem. 2 (2000) 2565.
[15] V. Lebarbier, G. Clet, M. Houalla, J. Phys. Chem. B 110 (2006) 22608.
[16] M.A. Cortés Jacome, M. Morales, C. Angeles Chavez, L.F. Ramirez Verduzco, E. López Salinas, J.A. Toledo Antonio, 2007, submitted for publication.
[17] T. Kasuga, M. Hiramatsu, A. Hoson, T. Sekino, K. Niihara, Langmuir 14 (1998) 3160.
[18] G.H. Du, Q. Chen, R.C. Che, Z.Y. Yuan, L.M. Peng, Appl. Phys. Lett. 79 (2001) 3702.
[19] R. Tenne, Nature 431 (2004) 640.
[20] R. Tenne, Angew. Chem. Int. Ed. 42 (2003) 5124.
[21] D.V. Bavykin, J.M. Friedrich, F.C. Walsh, Adv. Mater. 18 (2006) 2807.
[22] X. Chen, S.S. Mao, J. Nanosci. Nanotechnol. 6 (2006) 906.
[23] S. Loridant, C. Feche, N. Essayem, F. Figueras, J. Phys. Chem. B 109 (2005) 5631.
[24] M.A. Cortés-Jácome, G. Ferrat-Torres, L.F. Flores Ortiz, C. Angeles-Chávez, E. López-Salinas, J. Escobar, M.L. Mosqueira, J.A. Toledo-Antonio, Catal. Today 126 (2007) 248.
[25] D.V. Bavykin, J.M. Friedrich, A.A. Lapkin, F.C. Walsh, Chem. Mater. 18 (2006) 1124.
[26] M.A. Cortes-Jacome, C. Angeles-Chavez, X. Bokhimi, J.A. Toledo, J. Solid State Chem. 179 (2006) 2663.
[27] M.A. Cortes-Jacome, C. Angeles-Chavez, X. Bokhimi, J.A. Toledo, Appl. Catal. A 318 (2007) 178.